

## RESEARCH ARTICLE

# Hydrogel composition and laser micropatterning to regulate sciatic nerve regeneration

Yulia Berkovitch<sup>1,2</sup> | Talia Cohen<sup>3</sup> | Eli Peled<sup>3,4</sup> | Robert Schmidhammer<sup>5</sup> | Hildner Florian<sup>5</sup> | Andreas H. Teuschl<sup>5,6</sup> | Susanne Wolbank<sup>5</sup> | Dvir Yelin<sup>1</sup> | Heinz Redl<sup>5</sup> | Dror Seliktar<sup>1</sup> 

<sup>1</sup>The Faculty of Biomedical Engineering, Technion-Israel Institute of Technology, Haifa, Israel

<sup>2</sup>The Interdisciplinary Program for Biotechnology, Technion-Israel Institute of Technology, Haifa, Israel

<sup>3</sup>The Faculty of Medicine, Technion-Israel Institute of Technology, Haifa, Israel

<sup>4</sup>Orthopedic Surgery Division, Rambam Health Care Campus and The Bruce Rappaport Faculty of Medicine, Technion-Israel Institute of Technology, Haifa, Israel

<sup>5</sup>Ludwig Boltzmann Institute for Experimental and Clinical Traumatology, Austrian Cluster for Tissue Regeneration, Vienna, Austria

<sup>6</sup>Department of Biochemical Engineering, University of Applied Sciences Technikum Wien, Vienna, Austria

## Correspondence

Dror Seliktar, Technion-Israel Institute of Technology, Faculty of Biomedical Engineering, Technion City, Haifa 32000, Israel.  
Email: dror@bm.technion.ac.il

## Funding information

Russel Berrie Nanotechnology Institute; European Commission FP7, Grant/Award Number: BIODESIGN; Lorry I. Lokey Interdisciplinary Center for Life Sciences and Engineering

## Abstract

Treatment of peripheral nerve injuries has evolved over the past several decades to include the use of sophisticated new materials endowed with trophic and topographical cues that are essential for in vivo nerve fibre regeneration. In this research, we explored the use of an advanced design strategy for peripheral nerve repair, using biological and semi-synthetic hydrogels that enable controlled environmental stimuli to regenerate neurons and glial cells in a rat sciatic nerve resection model. The provisional nerve growth conduits were composed of either natural fibrin or adducts of synthetic polyethylene glycol and fibrinogen or gelatin. A photo-patterning technique was further applied to these 3D hydrogel biomaterials, in the form of laser-ablated microchannels, to provide contact guidance for unidirectional growth following sciatic nerve injury. We tested the regeneration capacity of subcritical nerve gap injuries in rats treated with photo-patterned materials and compared these with injuries treated with unpatterned hydrogels, either stiff or compliant. Among the factors tested were shear modulus, biological composition, and micropatterning of the materials. The microchannel guidance patterns, combined with appropriately matched degradation and stiffness properties of the material, proved most essential for the uniform tissue propagation during the nerve regeneration process.

## KEYWORDS

biomaterials, fibrinogen, hydrogels, micropatterning, nerve regeneration, nerve guidance conduit

## 1 | INTRODUCTION

Peripheral nerve damage, which is most often caused by trauma, is a serious problem in the medical community (Isaacs, 2013). Most efforts of restoration following severe nerve injury, particularly in the central nervous system, but also in the peripheral nervous system, are limited by an inability to fully control local cellular events using artificial devices. Therefore, most new technologies that aim to help facilitate regeneration following acute nerve injury are premised on a better understanding of nerve fibre formation in vivo. Natural repair does occur in a minority of peripheral nerve injuries. For example, if the nerve stumps have been displaced by a small gap, the nerve can often exhibit spontaneous repair whereby the axons regenerate into the columns of the Schwann cells to reconnect the nerve ends (Schmidt & Leach, 2003; Shoichet, Tate,

Baumann, & LaPlaca, 2008). However, when the displacement of the nerve stumps is more severe—as the case for larger gaps—the axons do not invade and the regeneration process cannot culminate into a functional neuronal tissue. In such cases, a surgical approach is needed to form an end-to-end anastomosis, or in more severe cases, autologous nerve grafting is required. Nerve auto-graft implantation causes loss of function at the harvest site and prolongs the operation or can even require more than one surgery. Therefore, alternative treatments are sought to help repair displaced nerve stumps (Schmidt & Leach, 2003).

One alternative to auto-graft nerve tissue is the use of nerve guidance conduits (NGCs). These materials-based technologies are clinically approved and hold a number of advantages over auto-grafting, including reduced collateral sprouting, limited myofibroblast infiltration, reduced neuroma and scar formation, and no associated donor site morbidity

(Kehoe, Zhang, & Boyd, 2012). The NGCs are also known to cause accumulation of a high concentration of neurotrophic factors which can improve axonal sprouting and nerve repair (Daly, Yao, Zeugolis, Windebank, & Pandit, 2012). Despite early clinical success with NGCs, their clinical efficacy is most pronounced with small injuries. However, understanding the regenerative process occurring within NGCs can help in the design of new NGC materials that improve upon the clinical outcomes for larger injuries. In this context, there have been many efforts in developing advanced materials for NGCs in order to stimulate regeneration of nerves following injury. Natural or synthetic materials are typically chosen on the basis of their capacity to facilitate a directional axonal sprouting. NGC materials support the survival of the cells and the regeneration process by providing physical and/or biological environmental cues (Bellamkonda, 2006; Sarig-Nadir, Livnat, Zajdman, Shoham, & Shoham, 2009; Teuschl et al., 2015). Recent strategies have tried to mimic the signals that direct embryonic nerve development, or nerve fibre regeneration following injury, as part of the design of the NGC material. These cues include spatiotemporal recruitment of neurotropic factors, extracellular matrix interactions, and cell-cell communications (Bellamkonda, 2006).

In this study, we apply natural and semi-synthetic biodegradable materials to create NGCs for peripheral nerve repair. We tested these NGCs in an 8-mm and 12-mm rat sciatic nerve resection model. The semi-synthetic approach provides us control features over the material properties, including shear modulus and degradation rate, without compromising the bioactivity of the materials, which is inherent to the biological extracellular matrix (ECM) constituent. The control features and bioactivity can in turn influence the physical and biological properties of the nerve tube in ways that are important for entubulation repair, including permeability, flexibility, swelling, degradation, and chemotaxis. The study compares three NGC materials, including natural fibrin, semi-synthetic fibrinogen-poly(ethylene glycol; PEG) adducts (PEG-Fib), and semi-synthetic gelatin-PEG adducts (PEG-Gel). The natural fibrinogen or gelatin components provide cues that can regulate neurite invasion, Schwann cell migration, and proliferation for promoting remyelination of the regenerated axons (Platt, Krekoski, Ward, Edwards, & Gavrilovic, 2003; Ryu, Davalos, & Akassoglou, 2009). The synthetic PEG component provides control over mechanical properties and degradation characteristics (Berdichevski, Shachaf, Wechsler, & Seliktar, 2015; Berkovitch & Seliktar, 2017; Dikovsky, Bianco-Peled, & Seliktar, 2006; Gonen-Wadmany, Goldshmid, & Seliktar, 2011). In addition, microchannels were inscribed using a photo-ablation technique in order to target reinnervation with limiting dispersion of regenerating axons (Berkovitch, Yelin, & Seliktar, 2015; Sarig-Nadir et al., 2009). The combination of controlled bioactivity, controlled physical characteristics, and uniaxial spatial patterns may ultimately provide us with an ideal NGC for regenerating peripheral nerves.

## 2 | MATERIALS AND METHODS

### 2.1 | Fibrinogen PEGylation

PEG-diacrylate (PEG-DA) was prepared from linear PEG-OH MW = 10 kDa (Fluka, Buchs, Switzerland) as described elsewhere (Almany & Seliktar, 2005). The conjugation of PEG to fibrinogen (i.e.,

PEGylation) was performed according to a protocol similar to the one described in detail by Dikovsky et al. (Dikovsky et al., 2006). Briefly, Tris (2-carboxyethyl) phosphine hydrochloride (Sigma-Aldrich) was added to a 7-mg/ml solution of bovine fibrinogen (MP Biomedicals, Solon, OH, USA) in 150-mM phosphate buffered saline (PBS) with 8 M urea (molar ratio 1.5:1 tris (2-carboxyethyl) phosphine to fibrinogen cysteines). Linear 10-kDa PEG-DA was reacted with the protein at a 4:1 molar ratio of PEG to fibrinogen cysteines for 3 hr. The PEG-fibrinogen (PEG-Fib) conjugate was precipitated in acetone and redissolved in PBS containing 8-M urea to 10- to 12-mg/ml final protein concentration. Then, the conjugate was dialysed against PBS at 4 °C for 1 day (Spectrum, 12–14 kDa MW cut-off, California, USA), sterilized and characterized according to previously published protocols (Dikovsky et al., 2006). The protein concentration was determined using a bicinchoninic acid Protein Assay (Pierce Biotechnology, Inc., Rockford, IL). To establish the total PEG-protein concentration, 0.5 ml of the precursor solution was lyophilized overnight and weighed. The amounts of total PEGylated product (dry weight) and protein content (bicinchoninic acid result) were used to calculate the PEG concentration in the precursor solution (Mironi-Harpaz, Berdichevski, & Seliktar, 2014). The final hydrogel precursor solution was prepared by diluting the PEG-Fib precursor to 8-mg/ml protein, and adding linear 10-kDa PEG-DA to the solution to reach 25-, 30- or 40-mg/ml PEG final concentrations (Table 1). These precursor solutions were supplemented with 0.1% (w/v) photo-initiator, Irgacure®2959 (Ciba Specialty Chemicals, Basel, Switzerland/Tarrytown, New York; Mironi-Harpaz, Wang, Venkatraman, & Seliktar 2012). The formation of a hydrogel was accomplished by photo-polymerization of the PEG-Fib solution under long-wave UV light (365 nm, 4–5 mW/cm<sup>2</sup>) exposure for 5 min (Schmidt, Mizrahi, Elisseeff, & Seliktar, 2006).

### 2.2 | Gelatin PEGylation

Thiolation of gelatin (Gelatin A, Porcine skin, Sigma) was accomplished using succinimidylacetyl-thioacetate (SATA, Pierce, Illinois, USA) based on the protocols described by Chen, Noah, Pallua and Steffens (2002) and further modified according to Berkovitch et al. (2015). Briefly, gelatin was dissolved in 150-mM PBS with 8-M urea at a concentration of 7 mg/ml. SATA was reacted for 2 hr at pH 7.5 and 37 °C with agitation (molar ratio 61:1 SATA to gelatin). The resulting acetylated SH groups on the lysine residues were deprotected by reacting 0.5-M hydroxylamine hydrochloride (NH<sub>2</sub>OH-HCL, Sigma-Aldrich) at a double molar ratio to the accepted acetylates, and PEGylated with 10-kDa PEG-DA (molar ratio 1.5:1 PEG-DA to incorporated thiols) at 37 °C with agitation for 3 hr. The PEG-gelatin (PEG-Gel) was precipitated in acetone at 37°C and redissolved in PBS with 8-M urea to 10- to 12-mg/ml final protein concentration and dialysed against PBS at 37 °C for 1 day (Spectrum, 12–14 kDa MW cut-off, California, USA). The conjugate was sterilized and characterized using the same procedure as for the PEG-Fib. The final hydrogel precursor solution was prepared with 8-mg/ml gelatin, 33-mg/ml PEG-DA, and 0.1% (w/v) photo-initiator, Irgacure®2959 (Ciba Specialty Chemicals,). The hydrogel crosslinking was accomplished as described for the PEG-Fib material (Schmidt et al., 2006).

**TABLE 1** Treatment cohorts

Group	Treatment	Protein composition	PEG-DA composition	Storage shear modulus (Pa)	Number of animals
I	Fibrin mixed with PEG-DA	50-mg/ml fibrin	25 mg/ml	n/a <sup>a</sup>	3
II	Fibrin only	50-mg/ml fibrin	0	1,130	3
III	Stiff PEG-fibrinogen	8-mg/ml fibrinogen	40 mg/ml	3,157	3
IV	Compliant PEG-fibrinogen	8-mg/ml fibrinogen	25 mg/ml	1,190	6
V	PEG-gelatin	8-mg/ml gelatin	33 mg/ml	108	6
VI	Micropatterned PEG-Fib	8-mg/ml fibrinogen	30 mg/ml	1,860	6
VII	Saline	n/a	n/a	n/a	6
VIII	Unoperated (wild-type)	n/a	n/a	n/a	n/a

Note. Various parameters for the treatments of the study design are detailed. The compositions of synthetic and protein constituents are given along with the shear storage modulus values of the materials and the number of animals tested in each cohort. PEG = poly(ethylene glycol); PEG-DA = PEG-diacrylate; PEG-Fib = PEG-fibrinogen.

<sup>a</sup>The shear storage modulus of Group I materials was not possible to obtain because of the rapid cross-linking that occurs when the constituents are mixed together

### 2.3 | Rheological characterization

Rheological measurements were carried out using a TA Instruments AR-G2 rheometer (ARES, TA Instruments, New Castle, DE, USA) equipped with a parallel-plate geometry and UV curing cell as described elsewhere (Mironi-Harpaz et al., 2012). Dynamic time sweep tests were performed at 37 °C, at a constant frequency of 3 rad/s and a sinusoidal 2% strain for 10 min to monitor the in situ gelation of the hydrogel precursor solutions (200  $\mu$ l) during the photo-polymerization reaction. After a 30-s preconditioning cycle, the precursor solutions were polymerized in the rheometer by exposing to long-wave UV light (365 nm, 5 mW/cm<sup>2</sup>) while the storage ( $G'$ ) and loss ( $G''$ ) modulus values were continuously recorded with RSIS Orchestrator 6.5.8 software (TA Instruments). The reported shear modulus was taken as the real part of the complex shear modulus  $G^* = G' + iG''$  at the conclusion of the test based on the rationale that the loss modulus was negligible in comparison to storage modulus of each sample.

### 2.4 | Nerve guidance conduit fabrication

Five different NGC material formulations were chosen for the in vivo regeneration studies as further detailed in Table 1. Two formulations were composed of fibrin, either mixed with PEG-DA (fibrin/PEG-DA) or fibrin alone (Groups I and II, respectively). The fibrin constructs were prepared from TissucolDuo 500 Fibrin Sealant (Baxter AG, Vienna, Austria) comprising thrombin concentrations of 4 IU/mL. Fibrinogen and thrombin were reconstituted according to the manufacturer's protocol. In brief, lyophilized sealer protein component of Tisseel was reconstituted in 3,000 KIE/mL aprotinin solution; the lyophilized thrombin component was reconstituted in 40 mM CaCl<sub>2</sub> solution. For in vivo clot formation, equal volumes of fibrinogen and thrombin components were mixed to initiate the clotting cascade. The fibrin with PEG-DA samples was similarly prepared with 2.5% (w/v) unreacted PEG-DA, having the precursor solution polymerized by exposing to long-wave UV light (365 nm, 5 mW/cm<sup>2</sup>) for 5 min. Two groups of PEG-fibrinogen (PEG-Fib) having different moduli were prepared by adding different amounts of PEG-DA crosslinker. These include a stiff PEG-Fib construct (Group III, 40 mg/ml PEG-DA) and a compliant

PEG-Fib construct (Group IV, 25-mg/ml PEG-DA). A PEG-Gel construct was prepared with 33-mg/ml PEG-DA crosslinker (Group V). Additionally, a micropatterned PEG-Fib construct was prepared with 30 mg/ml PEG-DA (Group VI). All treatments were compared with saline and unoperated (wild-type) controls (Groups VII and VIII, respectively). To fabricate the NGCs, each hydrogel precursor solution was injected into a long silicone tube mold with a 1.5- or 2-mm inner diameter, and cross-linked according to methods that were previously described (Berkovitch et al., 2015).

### 2.5 | Microchannel fabrication

Laser photoablation was used to generate guidance structures in the PEG-Fib hydrogels (Group VI). Briefly, the hydrogels were polymerized inside 10-mm long and 1.5-mm inner diameter silicone tubes. The gels were removed from the tube and preincubated in PBS solution overnight. Microchannels were ablated within the hydrogels using a commercial laser microdissector (P.A.L.M. MicroBeam system, Carl Zeiss MicroImaging GmbH, Bernried, Germany) set with a 20 $\times$  objective and motorized microscope stage (Berkovitch et al., 2015; Sarig-Nadir et al., 2009). Using a 1.35-mm beam diameter, the irradiance of the pulse train (355 nm wavelength, 1 ns pulse duration, 3pJ per pulse, and 100 Hz repetition rate) at the 2.6  $\mu$ m diameter focal spot was approximately  $4.5 \times 10^4$  W/cm<sup>2</sup>. Beam scanning speed across the sample was 100  $\mu$ m/s, resulting in a small 40% overlap between the spots of adjacent illumination pulses. The laser pulse energy was adjusted to produce channels with diameter of approximately  $70 \pm 5$   $\mu$ m (Berkovitch et al., 2015). Nineteen channels were ablated in each tube, with a distance of 200  $\mu$ m between channels according to the cross-sectional pattern shown in Figure 1.

### 2.6 | Animals studies and surgical procedure

All surgical and animal care procedures were carried out with approval from and in accordance with the Technion guidelines of the experimental animal committee. Adult male Lewis rats (150–250 g; Harlan, Israel) were housed in group cages, maintained on a 12-hr light/12-hr dark cycle, and food and water were available ad libitum. The rats were randomly assigned to the different groups, up to six animals in each group

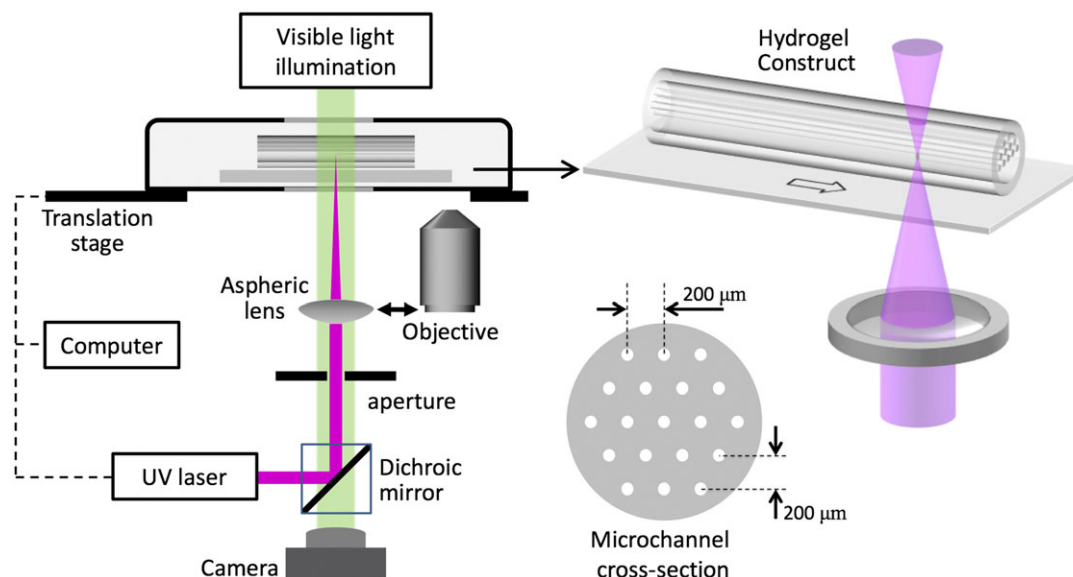


**FIGURE 1** The experimental setup for the laser-based microscopic ablation of poly(ethylene glycol)-protein hydrogels shows the various components of the optical system, including the beam focusing optics and hydrogel construct shown in a close-up view. The typical microchannel cross-section is shown in close-up view; 19 channels were ablated in each tube, with a distance of 200  $\mu\text{m}$  between channels [Colour figure can be viewed at [wileyonlinelibrary.com](http://wileyonlinelibrary.com)]

for every NGC treatment group. Rats were anaesthetized with an intramuscular injection of Ketamine (90 mg/kg) and Xylazine (10 mg/kg). The animals were shaved and the surgical area was cleaned with 70% ethanol. All procedures were performed under aseptic conditions. The sciatic nerve was exposed by a skin incision along the femur, followed by the separation of the biceps femoris and superficial gluteal muscles. An 8-mm or 12-mm nerve segment of the sciatic nerve was resected at the mid-thigh level, proximal to the tibial and peroneal bifurcation. After transection, 1 mm of the proximal and distal nerve stumps was sutured to the 10-mm or 14-mm long silicone tube (1.5- or 2-mm diameter) of randomly chosen nerve conduit to create an 8-mm or 12-mm nerve gap, respectively. For groups of rats assigned to fibrin, fibrin/PEG-DA, PEG-Fib, and PEG-Gel NGC treatments, the hydrogel precursor was injected into the silicone tube and polymerized either by thrombin (for the fibrin and fibrin/PEG-DA) or by in situ UV photochemistry to bridge the entire nerve gap after the tube was sutured to the proximal and distal stumps. For the group of rats assigned to PEG-Fib with microchannels, the NGC was fabricated ex situ in advance as described above. The nerve stumps were attached to the prefabricated NGC and sutured to the silicone tube. The incision site was sutured in layers with 3-0 Vicryl for muscle tissues and 3-0 silk sutures for skin. The animals were observed daily to check for signs of recovery. After set time-points, the rats were sacrificed with  $\text{CO}_2$  inhalation, and the NGC containing proximal and distal sciatic nerve segments was removed (Figure 2).

## 2.7 | Histology, immunofluorescence and confocal microscopy

The scaffolds were harvested, collected, and isolated from adhered muscle tissue. Afterwards, the silicone support tube was removed, and the tissue was fixed in 4% paraformaldehyde (Gadot, Haifa, Israel) and washed with PBS solution. Frozen

sections (10  $\mu\text{m}$ ) were either stained with haematoxylin and eosin (H&E), Masson's tri-chrome, or labelled with primary antibodies against  $\beta$ III-tubulin (G712A, Promega, Madison, WI, USA, 1:2000 dilution) and against S100 (S2644, Sigma, St. Louis, MO, USA, 1:200 dilution). Primary antibodies were subsequently labelled with fluorescently-conjugated secondary antibodies, including goat anti-mouse Cy3 (Chemicon International, Temecula, CA, USA; 1:250 dilution) and goat anti-rabbit Alexa 647 antibody (Chemicon International, Temecula, CA, USA; 1:400 dilution). A nuclear DAPI counter-stain was incorporated directly into the secondary antibody solution. The sections were imaged with a LSM700 scanning confocal microscope (Carl Zeiss Microscopy GmbH, Göttingen, Germany) using a 40 $\times$  objective.

## 2.8 | Statistical analysis

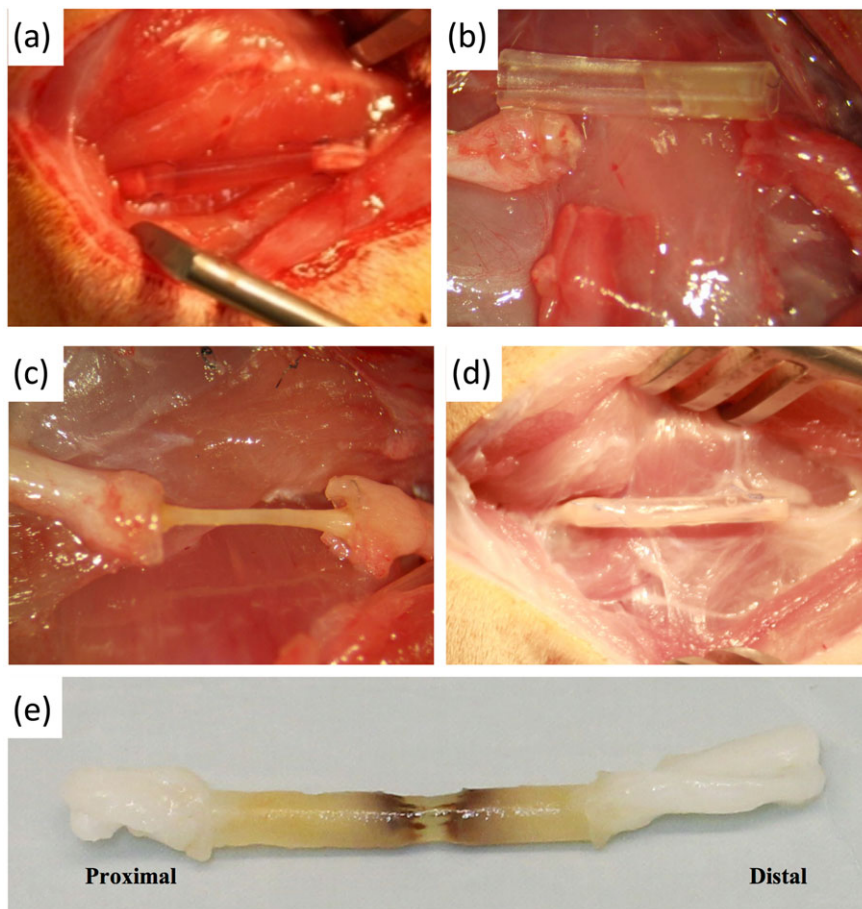
Statistical analysis was performed using Excel software (Microsoft Corporation, Redmond, WA, USA) or MATLAB software (MathWorks, Natick, MA, USA). Data from independent experiments were quantified and analysed for each variable. Comparisons between two treatments were made using Student's *t*-test (two-tailed, unequal variance) and comparisons between multiple treatments were made by one-way analysis of variance (ANOVA). A *p* value of  $<.05$  was considered to be statistically significant.

## 3 | RESULTS AND DISCUSSION

### 3.1 | Pilot feasibility study

For preliminary efficacy evaluation of the fibrin and PEG-Fib hydrogel materials in peripheral nerve regeneration, we commenced a pilot feasibility study with a common nerve injury model in the rat. The model consisted of a crush injury and resection of an 8-mm or

**FIGURE 2** The rat sciatic nerve injury model. During implantation, the proximal and distal nerve stumps are pulled into the lumen of the supporting silicone tube to create the nerve guidance conduit. The silicone tube is sutured and filled in with the hydrogel precursor solution, the precast hydrogel, or the saline solution. (a) Shown is a compliant poly(ethylene glycol)-fibrinogen (PEG-Fib) hydrogel on Day 0, with an inner diameter of 1.5 mm and a gap length of 12 mm. (b) Representative sample from Group I (fibrin/PEG-diacrylate hydrogel) shows the unbridged nerve gap on Week 12, with an inner diameter of 2 mm and a gap length of 8 mm. (c) Representative specimens from Group III (stiff PEG-Fibrin hydrogel) shows the bridged nerve gap on Week 12, with an inner diameter of 2 mm and a gap length of 8 mm. After removing the silicone conduit, the regenerated nerve tissue between the proximal and distal nerve stumps apparently has a smaller diameter. (d) Representative sample from Group IV (compliant PEG-Fib hydrogel) shows the bridged nerve gap on Week 7, with an inner diameter of 2 mm and a gap length of 8 mm; regenerated nerve tissue was evident within the silicone conduit. (e) Representative explanted sample from Group VI (micropatterned PEG-Fib hydrogel) shows the bridged nerve gap on Week 2, with an inner diameter of 2 mm and a gap length of 8 mm; regenerated nerve tissue was evident [Colour figure can be viewed at [wileyonlinelibrary.com](http://wileyonlinelibrary.com)]



12-mm length of the sciatic nerve, creating a subcritical gap (Lee, et al., 2003). A silicone supporting tube was sutured to the nerve stumps and filled with the matrix according to the conduit technique (Lee et al., 2003). The conduit technique is similar to the clinical paradigm of nerve repair using artificial nerve conduits (Fields, Le Beau, Longo, & Ellisman, 1989). The silicone tube is nondegradable and remains permanently in the host, but does not impeded upon the repair process that occurs in the internal compartment of the tube. The main purpose of the tube is to confine the scaffolding or matrix used for nerve regeneration in a direct line from the proximal to distal nerve stumps, but it also protects newly regenerated nerve fibres from scar invasion (Battiston, Geuna, Ferrero, & Tos, 2005).

Five compositions were examined for NGC efficacy as detailed in Table 1. Each NGC composition was tested in vivo with up to six replicates. Routine follow-up after surgery was performed, and the physical condition of treated hind limb was documented. No abnormal behaviour was observed in any of the animals. The rats dragged their hind-limb and their paw was curved. The muscle tissue loss associated with the operated limb was evident in all treatments. The site of injury is shown directly after implantation (Figure 2a), and the excision site is shown at the time of sacrifice for the different NGC compositions (Figure 2b–d). Some of the NGCs exhibited complete bridging of the nerve injury in as little as 2 weeks, whereas other NGCs exhibited only partial bridging even after 16 weeks, depending on the composition of

the matrix used. Both fibrin-based treatments (Groups I and II) did not manage to bridge the nerve injury (Figure 3). The fibrin mixed with PEG-DA treatment (Group I) degraded too slowly and thereby obstructed the regeneration of nerve tissue in the conduit (Figure 3). Visual inspection of this implant material after 12 weeks confirmed that the fibrin/PEG-DA hydrogel was present, but there was no sign of repair tissue in the confines of the silicone tube (Figure 2b). The fibrin only treatment (Group II) resulted in disorganized scar tissue in the injury site (Figure 3). Our results with the fibrin only were consistent with similar studies in which fibrin was shown to fall short of facilitating full nerve repair in a peripheral nerve injury model (Pettersson, Kalbermatten, McGrath, & Novikova, 2010).

Given the poor results obtained with natural fibrin-only materials, or the fibrin mixed with PEG-DA, we sought to evaluate a different formulation of fibrinogen and PEG as an NGC. We and others have shown that reconstituted fibrin is a suboptimal material for nerve repair partly owing to the mechanism of its clearance (Moy, 1988). Our hypothesis speculated that conjugating the fibrin(ogen) to PEG-DA would reduce these adverse effects, while still take advantage of the biodegradation and cell adhesive properties of the fibrinogen. The synthetic PEG-DA component of the system provides better control over the material properties and biodegradation characteristics of the matrix (Almany & Seliktar, 2005; Dikovskiy et al., 2006; Dikovskiy, Bianco-Peled, & Seliktar, 2010; Sarig-Nadir & Seliktar, 2008). Using

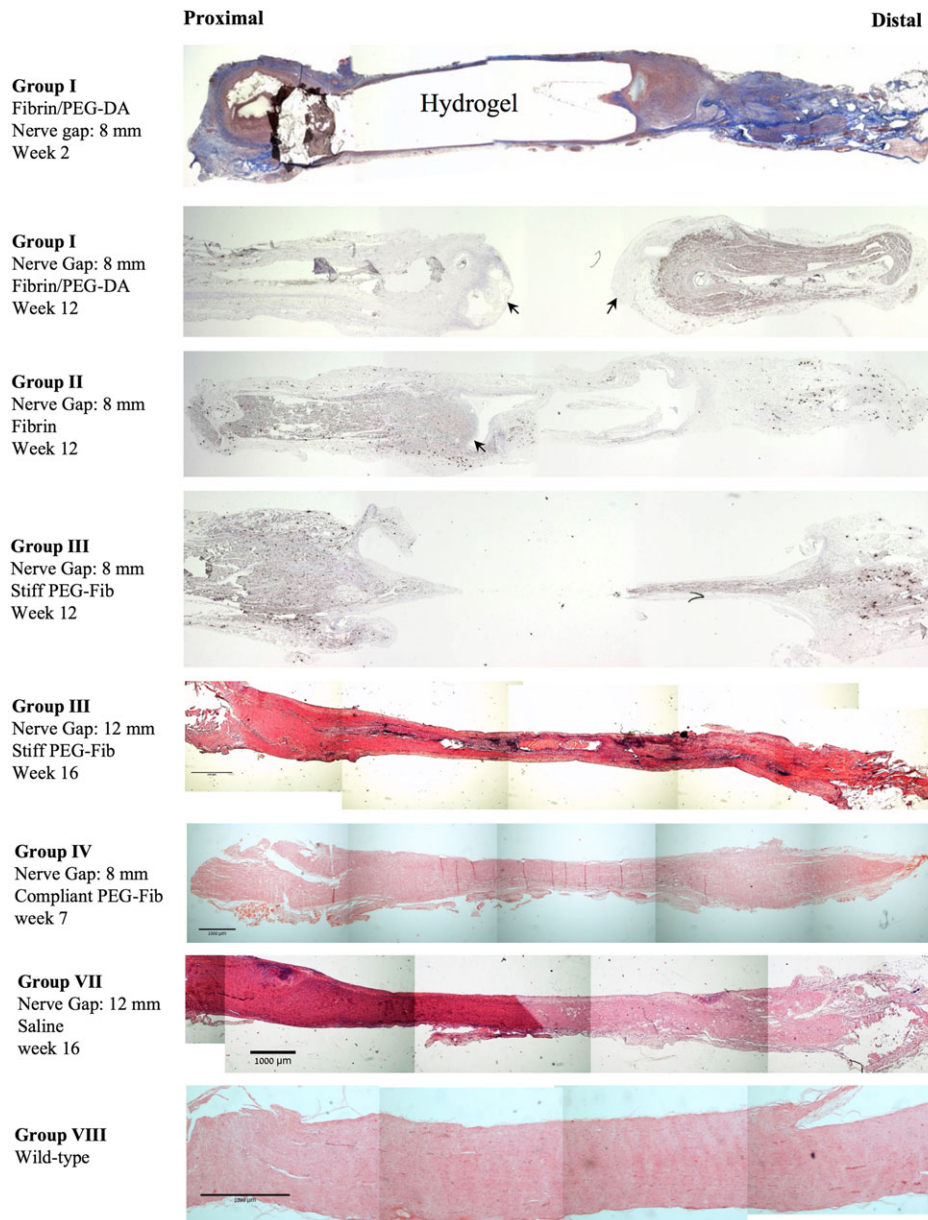


**FIGURE 3** Histological images of regenerated nerves from the feasibility study cohort. The histological characterization includes Masson's trichrome staining and haematoxylin and eosin staining of representative specimens of the regenerated sciatic nerve explants within a silicone tube filled with either fibrin, fibrin/poly(ethylene glycol)-diacrylate (PEG-DA), stiff poly(ethylene glycol)-fibrinogen (PEG-Fib), and compliant PEG-Fib after several weeks of repair. Saline control and wild-type tissue are also shown. In Group I, a region where the hydrogel remained intact prior to histological processing is labelled with the word "hydrogel." Arrows indicate the location of scar tissue formation. All micrographs show proximal side on left; follow-up times and injury dimensions are indicated next to the micrographs. Scale bar = 1,000  $\mu\text{m}$  [Colour figure can be viewed at [wileyonlinelibrary.com](http://wileyonlinelibrary.com)]

such control features, we have shown previously that the semi-synthetic hydrogels could better regulate neural cell outgrowth and survival, Schwann cell proliferation and overall nerve regeneration using an ex vivo model of nerve regeneration (Berkovitch & Seliktar, 2017; Sarig-Nadir & Seliktar, 2008, 2010). Thus, we prepared and tested three compositions of PEG-Fib hydrogels for sciatic nerve repair in the subcritical nerve gap: a compliant PEG-Fib, a stiff PEG-Fib, and a micropatterned PEG-Fib with microchannels. Together, these treatments were designed to examine the combined approaches of using controlled biodegradable matrices containing extracellular matrix proteins, and structurally aligned conduits, for peripheral nerve repair. The results with these NGCs indicated that the semi-synthetic

compositions can outperform fibrin and fibrin/PEG-DA, in bridging the nerve injury.

Our results indicate that the stiff PEG-Fib constructs containing 40-mg/ml PEG-DA (Group III) were better at promoting full bridging of the injury site compared with the fibrin/PEG-DA composition. Our earlier results with in vivo biodegradation of PEG-fib brought us to suspect that the composition-dependent biodegradation has something to do with this outcome (Peled, Boss, Bejar, & Seliktar, 2007). The results clearly indicate that the degradation of the fibrin/PEG-DA hydrogel was slower than the stiff PEG-Fib hydrogel, even though the fibrin/PEG-DA composition contained substantially lower concentrations of PEG-DA (25 mg/ml vs. 40 mg/ml for the stiff PEG-Fib). The

mixing of the PEG-DA with fibrin forms a nonenzymatically degradable double-network of PEG-DA and fibrin (Mironi-Harpaz, zigerson, & Seliktar, 2014), whereas the conjugation of the PEG-DA to the fibrinogen forms an enzymatically degradable PEG-Fib network where the *in vitro* degradation rate of the PEG-Fib is closely linked to the composition of PEG-DA in the matrix (Dikovskiy et al., 2010). Higher concentrations of PEG-DA resulted in greater cross-linking and slower degradation times (Berkovitch & Seliktar, 2017). Although in both systems, the amount of PEG-DA in the matrix controls the degradation rate of the material, the PEG-Fib retains an ability to undergo dissolution by enzymatic degradation, resulting in faster *in vivo* degradation. Hence, the PEG-Fib gives way faster for the bridging of the defect to occur (i.e., does not obstruct repair). Nevertheless, the rate of degradation of the stiff PEG-Fib was somewhat slow and did not facilitate full bridging in the 16 week recovery period. We therefore speculate that the composition-dependent *in vivo* degradation rate of the stiff PEG-Fib NGC was an impediment contributing to its limited repair outcomes. Specially, the repair tissue was significantly thinner than the adjacent proximal and distal nerve stumps (Figure 2c). Histological evaluation confirmed the limited diameter of the repair tissue in the stiff PEG-Fib treated animals, even after 16 weeks (Figure 3).

Further reducing the concentration of the PEG-DA crosslinker to 25 mg/ml in the PEG-Fib treatment (i.e., compliant PEG-Fib, Group IV) also reduced the degradation time of the implant and favorably affected the nerve repair process. Histological evaluation of samples from Group IV confirmed the bridging of the defect was evident by 7 weeks, with no signs of hydrogel remnants visible at this time point (Figures 3, and 4). Moreover, the diameter of the repair tissue in the compliant PEG-Fib treated samples after only 7 weeks was noticeably increased; although the implant was less uniform along its lateral axis (Figures 2d and 3). In contrast, the Group III implants made with PEG-Fib containing 40 mg/ml were not fully degraded even after 16 weeks, as evidenced by remaining hydrogel visible in cross-sections of the excised implants (Figures 3, and 4). Although the difference in degradation rate could be one of the contributing factors to the different repair outcomes (Sarig-Nadir & Seliktar, 2008, 2010), one cannot exclude the possibility that the lower modulus of the compliant PEG-Fib implant enhanced the invasion of neurites and Schwann cells into the NCG to accelerate the repair process in this treatment condition (Berkovitch & Seliktar, 2017).

Interestingly, the saline controls (Group VII) demonstrated comparable tissue repair in terms of the diameter at 16 weeks, when compared with compliant PEG-Fib at 7 weeks (Figure 3). However, the histological comparison shows less organization in the repair tissue of the saline control group, with fewer axially oriented lamella structures (Figure 4). High-magnification histological cross-sections of the repair tissue verified the observed trends in the NGC-treated explants and wild-type animals. Specifically, cross-section images of the compliant PEG-Fib treated explants reveal a highly vascularized repair tissue, with oriented lamellar structures organized throughout, even in the midsection of the explant (Figure 4). All the NGC treatments exhibited a thin fibrous tissue capsule external to the silicone tube walls. In contrast, the wild-type sciatic nerve tissue (Group VIII) was highly uniform and homogeneously populated with cells, without the fibrous capsule formation (Figure 4). We presume that the fibrous capsule is part of

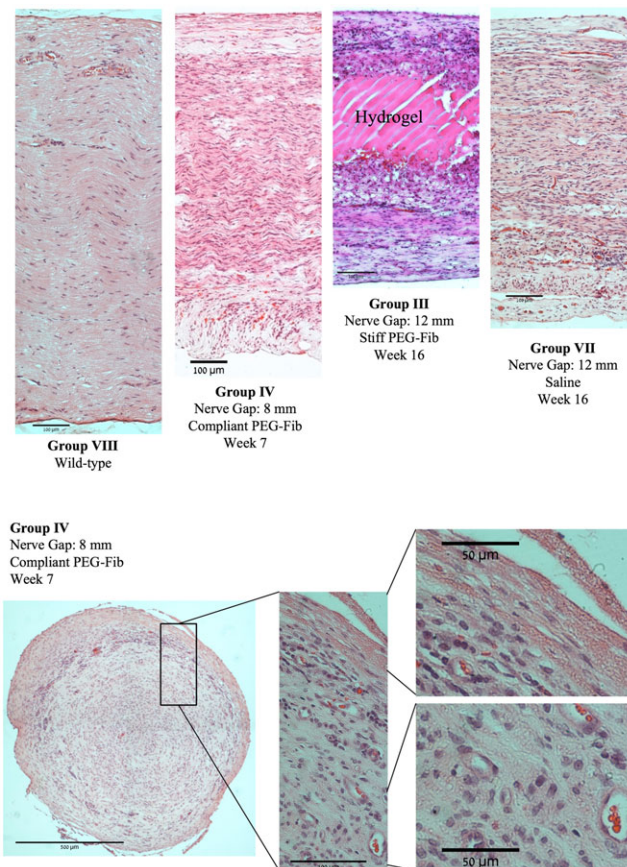


**FIGURE 4** High magnification histological images of regenerated nerves from the feasibility study cohort. Axial cross-sections of representative wild-type, compliant poly(ethylene glycol)-fibrinogen (PEG-Fib), stiff PEG-Fib, and saline treatment explants are shown with haematoxylin and eosin staining (top); scale bar = 100  $\mu$ m. In Group III, a region where the hydrogel remains intact is labelled with the word “hydrogel.” Transverse cross-section of the representative specimen from the compliant PEG-Fib treatment explant shows the orientation of the regenerated tissue, as well as evidence of angiogenesis as indicated by capillary formations deep within the new tissue [Colour figure can be viewed at [wileyonlinelibrary.com](http://wileyonlinelibrary.com)]

the normal host reaction following implantation of the silicone biomaterial (Anderson, Rodriguez, & Chang, 2008). In comparison to the wild-type tissue, the repair of all NGC-treated animals and saline control group were suboptimal (Figures 3, and 4).

### 3.2 | Subacute nerve repair study

Evidence from the pilot feasibility study helped to further refine our investigation of the initial (subacute) phase of the sciatic nerve repair process. Our pivotal study was limited to using the different protein compositions of PEG-protein adducts, while keeping other parameters constant, including the follow-up duration, segmental defect length, and diameter of the silicone tube. Given the poor performances of the fibrin, fibrin/PED-DA, and stiff PEG-Fib compositions, these treatments were not pursued, and further experiments were performed with compliant PEG-Fib and patterned PEG-Fib, as well as a PEG-gelatin hydrogel NGC. The use of a PEG-Gel material was introduced because of the rationale that, unlike fibrin, collagen based materials, including gelatin, may provide a better ECM repair substrate for nerve injuries

(Angius et al., 2012; Deal, Griffin, & Hogan, 2012; Sarig-Nadir & Seliktar, 2008). We also limited our follow-up evaluation to 2 weeks after the injury so as to enable a direct comparison during the subacute repair process for each treatment. Generally, nerve regeneration can be organized into five major phases that comprise the processes of regeneration following NGC placement: post-traumatic response; migration of cells and cell processes into the tube; differentiation of neuronal, glial, and vascular elements; axonal growth; and myelination (Fields et al., 1989). The subacute phases are mainly the post-traumatic response and the migration of cells; although some differentiation of neuronal, glial, and vascular elements can begin in this time-frame. The histological assessments that were chosen for evaluation were presumed to be most appropriate for the first two phases of the nerve regeneration.

There was no evidence of a local inflammatory response in any of the treated animals after 2 weeks. In NGCs comprising the compliant PEG-Fib (Group IV), PEG-Gel (Group V), and saline (Group VII), the regenerated tissue filled the inner lumen of the conduit after 2 weeks, thus bridging the 8-mm gap between the two nerve stumps. In addition to repair tissue, there was evidence of the formation of a thin fibrous tissue capsule adjacent to the silicone tube walls, which is the typical host reaction following implantation of a foreign body (Figure 4, Group IV). However, there was no evidence of hydrogel remnants within the repair tissue locale, suggesting that hydrogels undergo complete degradation during 2 weeks, thereby enabling reconnection of the two nerve stumps with repair tissue. As before, we observed a non-uniform repair tissue in the injury site, as evidenced by a decreased lumen diameter in the middle of the explants (Figure 5).

The immunofluorescence staining showed the presence of a diverse population of infiltrated cells in the repair tissue after 2 weeks, including glial cells and  $\beta$ III-tubulin positive neurites (Figure 5). Images of immunohistochemistry reveal multiple nuclei and low glia cell marker expression in midsections of the specimen, helping to differentiate the regenerated tissue from the healthy tissue at the nerve stumps (proximal region; Figures 5 and 6). The repair tissue was highly non-uniform as indicated by morphology of the nuclei and  $\beta$ III-tubulin cells. For example, they exhibited irregular morphologies when in close proximity to the distal end of the nerve stump. Longitudinal orientation of the tissue structures along the major axis of the NGC can be seen in PEG-Gel (Group V) treated animals; however, the PEG-Fib treatment (Group IV) and saline controls exhibited far less longitudinally aligned tissue structures. The saline control group also exhibited fewer glial cells in comparison to the PEG-Gel and PEG-Fib treatments.

### 3.3 | Micropatterned PEG-Fib NGCs

A micropatterned PEG-Fib material was used to investigate the nerve repair process in the subacute phase through an inhomogeneous material. We previously showed that such materials can be used to better control *ex vivo* neurite invasion and glial cell growth by contact guidance and ECM-like bioactivity (Berkovitch et al., 2015; Sarig-Nadir et al., 2009). The composition of the micropatterned PEG-Fib was modified slightly for this purpose—in comparison with the compliant PEG-Fib—by increasing the PEG-DA crosslinker to 30 mg/ml. The purpose for this change was to increase the stiffness of the material so as

to limit cellular infiltration into the bulk of the materials and maximize the infiltration into the micropatterned regions of the NGC (Berkovitch et al., 2015; Sarig-Nadir et al., 2009). The 2-week *in vivo* results with the micropatterned NGC were substantially different compared with the other treatments (Figure 6). For example, regions of axially oriented glial cells,  $\beta$ III-tubulin, and additional cell nuclei can be distinguished surrounded by non-oriented cells and tubulin proximal to the remaining PEG-Fib hydrogel. Furthermore, glial cells can be seen invading into the channels within the residual nondegraded PEG-Fib hydrogel. Around the channels, the remnant hydrogel stained non-specifically for  $\beta$ III-tubulin, perhaps owing to the incorporation of  $\beta$ III-tubulin protein into the matrix. From the distal nerve stump, a more disorganized tissue infiltrate was observed, as compared with the proximal side's tissue infiltrate. It also appeared that the propagation of new tissue from proximal nerve stump was occurring more expeditiously. Interestingly, the tissue infiltrate filled the entire tube diameter in the micropatterned NGCs, when compared with all the other NGC treatments. However, there was not a complete bridging of the nerve gap during the 2-week period of recovery (Figure 6). Consequently, microscopic evaluation of the implant still revealed the microchannels within the remaining hydrogel in the midsection of the explants.

We speculate that contact guidance of growing neurites was partly responsible for the tissue growth response into the microchannels (Dubey, Letourneau, & Tranquillo, 2001; Sherman & Brophy, 2005). In particular, the neurite projections appearing aligned in an axial direction inside the channels can be attributed to patterning of a relatively stiff hydrogel. It is likewise possible that the increased stiffness and slower degradation of the micropatterned PEG-Fib hydrogel supported invasion of neurites and glial cells into the channels whereas other cell types (endothelial cells and fibroblasts) degraded the surrounding hydrogel to eventually fill the entire nerve conduit lumen with mesenchymal tissue. These guidance channels in the PEG-Fib hydrogels can act somewhat similarly to the pathways created by a fibrin cable naturally formed between two nerve stumps in time of nerve regeneration in hollow conduits (Daly et al., 2012). We also hypothesize that the ablation of channels with the ultraviolet laser can better expose fibrinogen motifs responsible for cell adhesion, migration, and proliferation. Thus, by incorporating the fibrinogen into the micropatterned NGC, we may emulate and extend the critical step of acellular fibrin bands of Büngner formation, which typically lasts for 2–6 days (Daly et al., 2012), and gain more time for longer defects to repair as compared with hollow nerve guidance conduit. In this context, it was previously found that matrices of fibrin tend to have greater intrinsic strength and support for cell ingrowth from surrounding tissues than other protein scaffolds (Choi et al., 2005). However, there have been relatively few attempts to construct implantable fibrin scaffolds with controlled 3D architecture for NGCs, in part because of fibrin's potentially adverse effects on nerve repair (Herbert, Nagaswami, Bittner, Hubbell, & Weisel, 1998). Here, we have succeeded in creating patterned NGCs with biomimetic and controllable structures from fibrin(ogen)-based materials, which are promising for application of nerve injury repair.

One of the important parameters associated with nerve repair is the diameter of the repair tissue in the NGC. As a part of our results, we quantified the diameter of the repair tissue along the axial

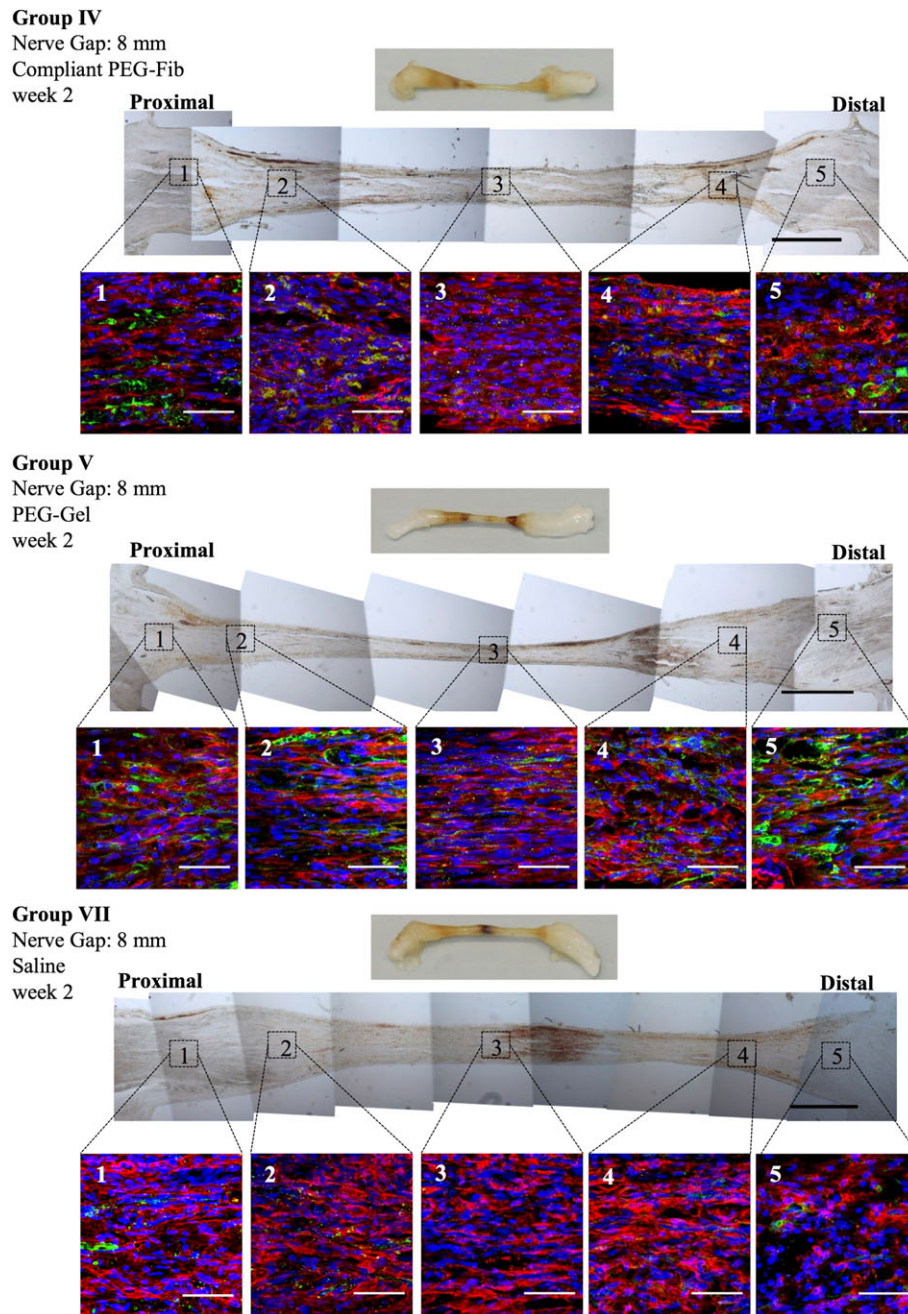


**FIGURE 5** Histological and gross images of regenerated nerves from the subacute study cohort. The histological characterization includes Masson's trichrome staining of representative specimens of the regenerated sciatic nerve explants within a silicone tube filled with either compliant PEG-fibrinogen (PEG-Fib), PEG-gelatin (PEG-Gel), or saline after 2 weeks of repair; scale bar = 1,000  $\mu$ m. The immunofluorescence characterization includes specific markers for neurons ( $\beta$ III-tubulin, red), glial cells (S100, green) and cell nuclei (4',6-diamidino-2-phenylindole, blue). Representative confocal microscopy images of axial positions along the specimen reveal distinct patterns of neural organization, glial cells organization as well as tissue organization; scale bar = 50  $\mu$ m [Colour figure can be viewed at [wileyonlinelibrary.com](http://wileyonlinelibrary.com)]

dimension of the NGC explants. The diameter of regenerated tissue within the silicone tube from the proximal to distal nerve stumps reveals a distinct narrowing of the tissue in the middle part of all NGCs tested, with the exception of the micropatterned PEG-Fib treatment (Figure 6). There were no significant differences in diameter between the saline and compliant PEG-Fib NGCs in this regard. However, the PEG-Gel treatment did exhibit a significant difference in diameter at the proximal side of the regenerated tissues ( $p < .05$ ,  $n = 6$ ). These significant differences were evident up until the middle of the NGC; approximately 4 mm inward from the proximal side. Beyond the middle

of the NGCs towards the distal nerve stump, there was no significant difference between saline, PEG-Fib and PEG-Gel treatments in terms of the infiltrated tissue diameter ( $p > .05$ ,  $n = 6$ ). In contrast to these treatments, the infiltration inside the micropatterned PEG-Fib treatment showed a frontal invasion from both proximal (approximately 4 mm) and distal (approximately 2.6 mm) nerve stumps (Figure 7), without an apparent narrowing of the regenerated tissue, and with significant differences to all other treatments at every location along the length of the NGC ( $p < .05$ ,  $n = 6$ ). It is important to note that the invasion described refers primarily to the glial invasion phase of repair. This

**Group VI**  
Nerve Gap: 8 mm  
Micro-patterned PEG-Fib  
week 2

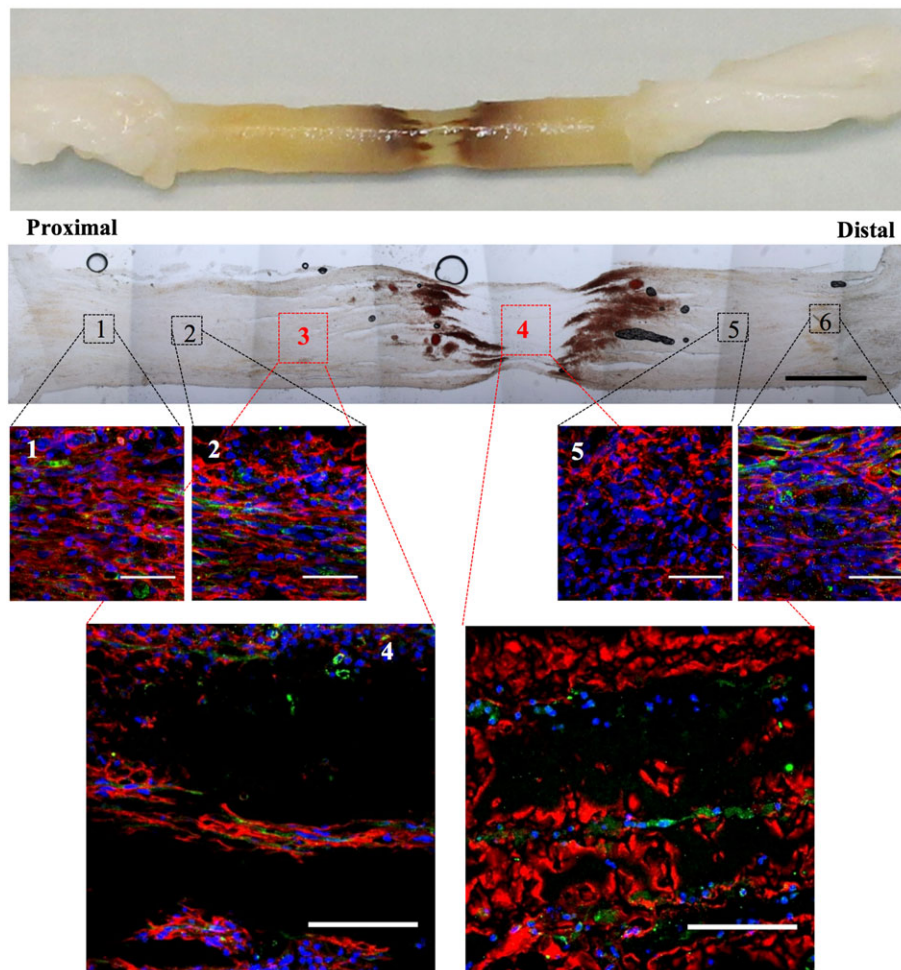


**FIGURE 6** Histological and gross images of regenerated nerves from the subacute study cohort. Representative explanted sample from the micro-patterned PEG-fibrinogen (PEG-Fib) hydrogel treatment (Group VI) shows the bridged nerve gap after 2 weeks, with an inner diameter of 2 mm and a gap length of 8 mm; regenerated nerve tissue was evident. The histological characterization includes Masson's trichrome staining of the representative specimen of the regenerated sciatic nerve explant without the silicone tube; scale bar = 100  $\mu$ m. The immunofluorescence characterization includes specific markers for neurons ( $\beta$ III-tubulin, red), glial cells (S100, green), and cell nuclei (4',6-diamidino-2-phenylindole, blue). Representative confocal microscopy images of axial positions along the specimen reveal distinct patterns of neural organization, glial cells organization as well as tissue organization; scale bar = 50  $\mu$ m. A schematic of the pattern of microchannel formation in cross-section is shown. The laser pulse energy was adjusted to produce channels with diameter 70  $\mu$ m. The channels were ablated with a distance 200  $\mu$ m between channels as indicated [Colour figure can be viewed at [wileyonlinelibrary.com](http://wileyonlinelibrary.com)]

does not infer the formation of mature nerve fibres or fully developed axonal structures associated with nerve fibre regeneration, which are expected to originate proximal to the lesion at later time-points (Battiston et al., 2005).

### 3.4 | Proposed mechanism of repair

We assume that the slightly more cross-linked micro-patterned PEG-Fib NGC remained partially intact—most noticeable in the middle of the nerve gap—and thereby allowed the NGC resorption to better synchronize with the infiltrating tissue. The other treatments exhibited a substantial narrowing of the regenerated tissue in the middle part of

the hydrogel treatments (Figure 5), which is very similar to nerve regeneration behaviour in a hollow conduit (Belkas, Shoichett, & Midha, 2004). We attribute the differences in repair patterns to the combined compliance, patterning, and degradation times of the different material compositions tested (Table 1 summarizes some of these parameters). Other studies with collagen filament conduits showed similar dependence of rat sciatic nerve regeneration on conduit packing density (Yoshii, Oka, Shima, Taniguchi, & Yoshii, 2003). Berkovitch and Seliktar (2017) provided evidence that matrix properties can affect axon regeneration in 3D hydrogels using an *in vitro* dorsal root ganglion model (Berkovitch & Seliktar, 2017). They found that axonal outgrowth was highly correlated with the density of different hydrogel

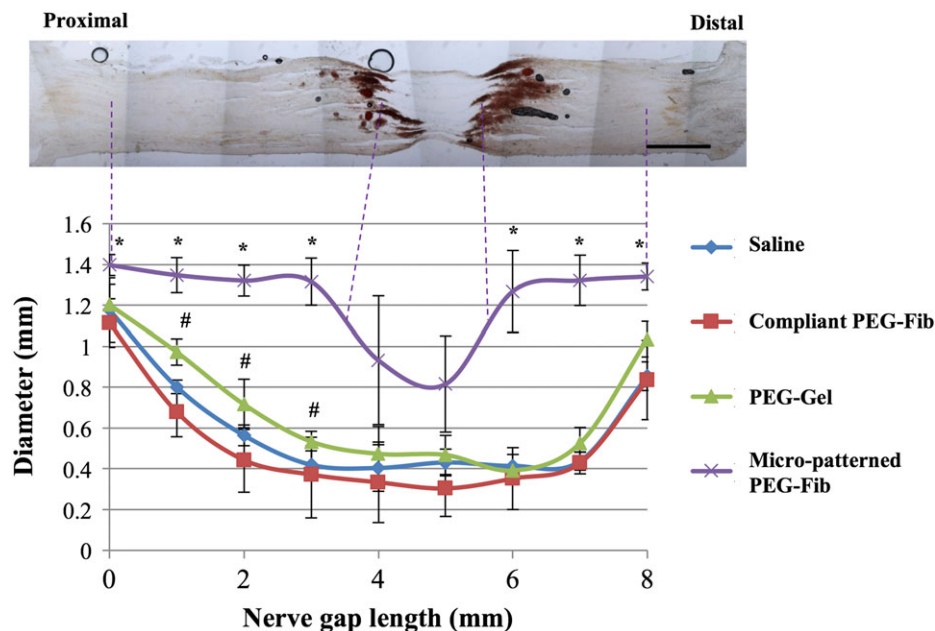


**FIGURE 7** Tissue regeneration as quantitatively measured by the diameter along the length of the explanted tissue specimen from the subacute study cohort after 2 weeks. The regenerated tissue diameter on the proximal side was significantly higher in the PEG-gelatin (PEG-Gel) treatment, when compared with the saline and compliant PEG-fibrinogen (PEG-Fib) treatments ( $p < .05$ ,  $n = 6$  for each group; # indicates significant differences between PEG-Gel and saline treatments). The distal end of the specimen showed no significant difference between the three samples PEG-Gel, saline, and compliant PEG-Fib treatments. The micropatterned PEG-Fib treatment exhibited significantly different diameter on both the proximal and distal ends of the regenerated tissue specimens ( $p < .05$ ,  $n = 6$ ; \* indicates significant differences between micropatterned PEG-Fib and saline treatments at the indicated axial location). The tissue ingrowth from both proximal and distal ends was homogenous, with hydrogel remnants observed in the midsection of the micropatterned specimens [Colour figure can be viewed at [wileyonlinelibrary.com](http://wileyonlinelibrary.com)]

compositions. Other studies showed similar findings regarding axonal growth and mechanical properties of the matrix, most notably the modulus (Athamneh & Suter, 2015).

Histological evaluation revealed infiltration of nerve tissue cells (glial cells) from both proximal and distal nerve stumps, and axial orientation of  $\beta$ III-tubulin positive fibres and elongation of cell nuclei along the NGCs was observed in the proximal side of newly regenerated nerves. In the compliant PEG-Fib treatment, this orientation is evident also in the distal stump of the nerve (Figure 5). Both treatments containing compliant protein-based materials comprise more glial cells compared with the saline control (Figure 5). The limited organization of the regenerated tissue in the middle of the NGC can be caused by rapid degradation and clearance of the support scaffold, possibly providing a limited ability to physically support neurites, glial cells, and other cells that are essential for this regeneration. We also consider the adhesion motifs of the ECM proteins in these materials to be an important contributing factor to the cell invasion results, although further investigations would be required to substantiate the importance of bioactivity of the ECM component in the repair process. Another approach to introduce specific bioactivity to NGCs is through the use of immobilized growth factors such as nerve growth factor (NGF). Lee et al. immobilized NGF into fibrin scaffolds in order to substantially improve nerve regeneration in a rat sciatic injury model (Lee et al., 2003). The PEG-Fib materials have also been endowed and tested ex vivo with NGF (Berkovitch & Seliktar, 2017; Sarig-Nadir & Seliktar, 2008, 2010) and in vivo with other growth factors for other indications (Berdichevski, Simaan Yameen, Dafni, Neeman, & Seliktar, 2015; Rufaihah et al., 2017; Rufaihah et al., 2013); however, a comprehensive

in vivo study of PEG-Fib with NGF for nerve injuries is warranted as part of our future validation of this strategy.

One of shortcomings of this study is the limited repair times that were chosen. We evaluated repair after 2 weeks to focus on the subacute phase. In general, nerve regeneration can take several months, proceeding along five main phases, including the initial fluid phase (first day), the formation of an acellular fibrin cable between the proximal and distal stumps (first week), formation of glial bands of Büngner (second week), the axonal phase of repair (2–4 weeks), and myelin sheath phase (6–16 weeks; Daly et al., 2012; Pettersson et al., 2010). The repair process in an NGC occurs in nerve gaps of up to 4 cm in humans and up to 1.5 cm in a rat sciatic nerve model (Belkas et al., 2004; Daly et al., 2012). Fibrin formation is a crucial step in this nerve regeneration. For example, if fibrin fails to form between the nerve stumps, as is the case when NGCs are used to repair large nerve gaps, the regeneration will not occur. Moreover, the uniformity of the fibrin clot can be influenced by the dimensions of the nerve gap; large nerve gaps tend to create fibrin clots that taper from nerve stumps towards the midregion of the injury (Belkas et al., 2004). More severe tapers will result in less uniform repair. Our study's focus on the phase of the formation of glial bands of Büngner was chosen to estimate how alternative fibrin-based NGC material compositions and their patterning are able to support nerve regeneration based on their stiffness, degradation, ECM composition, and contact guidance channels. Based on our results, we can conclude that structural features of the NGC, combined with appropriately matched material properties such as modulus or degradation rate, should be applied to avoid rapid resorption of the implant and provide physical support for axonal propagation.

Structurally aligned scaffolds with tubelike microtopography increase the effectiveness of regeneration only if the tubes maintain their structural integrity throughout their entire length (Spivey, Khaing, Shear, & Schmidt, 2012). The micropatterned PEG-Fib hydrogel containing microchannels fits this classification, mimicking the integrity of the endoneurial sheath (basal lamina) and efficiently guiding neurons across the peripheral nerve defect. The follow-up after 2-week recovery was essential for visualizing this aspect of the regeneration process. The longer-term healing evaluation—as well as functional outcome measurements—would not provide a proper snapshot of important events associated with structure and composition as pertaining to NGC nerve regeneration. However, these follow-up studies are essential to fully understand the entire process of nerve repair using this family of PEG-protein adducts as hydrogel materials for NGC.

## 4 | CONCLUSION

In this study, we applied a semi-synthetic hydrogel matrix possessing distinct biochemical, mechanical, and structural properties for studying the relative importance of certain components in affecting peripheral nervous system regeneration after injury. Fibrin, PEG-Fib, PEG-Gel, and PEG-Fib hydrogels with microchannels ablated longitudinally were applied as NGCs for sciatic nerve regeneration in a rat model, and compared with saline (hollow) NGC treatment. With exception of the fibrin treatments, all other NGCs tested supported some extent of nerve tissue restoration. The compliance and degradation of the hydrogel NGC matrix needs to be optimized to avoid narrowing of nerve tissue in the middle of the injury site, or to avoid obstructing the bridging repair process altogether. Microchannels in combination with optimized material properties provided the best template for nerve regeneration in our study. The structured scaffolds sustained the repair by leading and mediating contact guidance of neurites and adhesion-dependent migration of glial cells, without losing structural integrity as the newly regenerated sciatic nerve tissue replaced the provisional semi-synthetic matrix.

## ACKNOWLEDGEMENTS

This work was supported in part by the Lorry I. Lokey Interdisciplinary Center for Life Sciences and Engineering, Russel Berrie Nanotechnology Institute, as well as by the European Commission FP7 grant BIODESIGN.

## CONFLICT OF INTEREST

The authors have declared that there is no conflict of interest.

## AUTHOR CONTRIBUTIONS

Y. B. designed the experiments, performed in vitro experiments, performed animal surgeries, analysed data, and wrote the manuscript; N. C. performed animal surgeries and analysed the data; E. P. performed animal surgeries and analysed the data; R. S. performed animal surgeries and analysed the data; H. F. performed in vitro experiments and analysed the data; A. T. performed in vitro experiments, performed

animal surgeries, and analysed the data; S. W. performed in vitro experiments, performed animal surgeries, and analysed the data; D. Y. designed experiments, analysed the data, and wrote the manuscript; H. R. designed the experiments, analysed the data, and wrote the manuscript; and D. S. designed the experiments, analysed the data, and wrote the manuscript.

## ORCID

Dror Seliktar  <http://orcid.org/0000-0001-6964-8567>

## REFERENCES

- Almany, L., & Seliktar, D. (2005). Biosynthetic hydrogel scaffolds made from fibrinogen and polyethylene glycol for 3D cell cultures. *Biomaterials*, 26(15), 2467–2477.
- Anderson, J. M., Rodriguez, A., & Chang, D. T. (2008). Foreign body reaction to biomaterials. *Seminars in Immunology*, 20(2), 86–100.
- Angius, D., Wang, H., Spinner, R. J., Gutierrez-Cotto, Y., Yaszemski, M. J., & Windebank, A. J. (2012). A systematic review of animal models used to study nerve regeneration in tissue-engineered scaffolds. *Biomaterials*, 33(32), 8034–8039.
- Athamneh, A. I., & Suter, D. M. (2015). Quantifying mechanical force in axonal growth and guidance. *Frontiers in Cellular Neuroscience*, 9, 359.
- Battiston, B., Geuna, S., Ferrero, M., & Tos, P. (2005). Nerve repair by means of tubulization: Literature review and personal clinical experience comparing biological and synthetic conduits for sensory nerve repair. *Microsurgery*, 25(4), 258–267.
- Belkas, J. S., Shoichett, M. S., & Midha, R. (2004). Peripheral nerve regeneration through guidance tubes. *Neurological Research*, 26(2), 151–160.
- Bellamkonda, R. V. (2006). Peripheral nerve regeneration: An opinion on channels, scaffolds and anisotropy. *Biomaterials*, 27(19), 3515–3518.
- Berdichevski, A., Shachaf, Y., Wechsler, R., & Seliktar, D. (2015). Protein composition alters in vivo resorption of PEG-based hydrogels as monitored by contrast-enhanced MRI. *Biomaterials*, 42, 1–10.
- Berdichevski, A., Simaan Yameen, H., Dafni, H., Neeman, M., & Seliktar, D. (2015). Using bimodal MRI/fluorescence imaging to identify host angiogenic response to implants. *Proceedings of the National Academy of Sciences of the United States of America*, 112(16), 5147–5152.
- Berkovitch, Y., & Seliktar, D. (2017). Semi-synthetic hydrogel composition and stiffness regulate neuronal morphogenesis. *International Journal of Pharmaceutics*, 523(2), 545–555.
- Berkovitch, Y., Yelin, D., & Seliktar, D. (2015). Photo-patterning PEG-based hydrogels for neuronal engineering. *European Polymer Journal*, 72, 473–483.
- Chen, J. S., Noah, E. M., Pallua, N., & Steffens, G. C. M. (2002). The use of bifunctional polyethyleneglycol derivatives for coupling of proteins to and cross-linking of collagen matrices. *Journal of Materials Science: Materials in Medicine*, 13(11), 1029–1035.
- Choi, E. H., Han, S. G., Kim, S. H., Zhu, S. J., Huh, J. Y., Jung, J. H., ... Kim, B. Y. (2005). Autologous fibrin glue in peripheral nerve regeneration in vivo. *Microsurgery*, 25(6), 495–499.
- Daly, W., Yao, L., Zeugolis, D., Windebank, A., & Pandit, A. (2012). A biomaterials approach to peripheral nerve regeneration: Bridging the peripheral nerve gap and enhancing functional recovery. *Journal of the Royal Society Interface*, 9(67), 202–221.
- Deal, D. N., Griffin, J. W., & Hogan, M. V. (2012). Nerve conduits for nerve repair or reconstruction. *Journal of the American Academy of Orthopaedic Surgeons*, 20(2), 63–68.
- Dikovsky, D., Bianco-Peled, H., & Seliktar, D. (2006). The effect of structural alterations of PEG-fibrinogen hydrogel scaffolds on 3-D cellular morphology and cellular migration. *Biomaterials*, 27(8), 1496–1506.
- Dikovsky, D., Bianco-Peled, H., & Seliktar, D. (2010). Proteolytically degradable photo-polymerized hydrogels made from PEG-fibrinogen adducts. *Advanced Engineering Materials*, 12(6), B200–B209.

- Dubey, N., Letourneau, P. C., & Tranquillo, R. T. (2001). Neuronal contact guidance in magnetically aligned fibrin gels: Effect of variation in gel mechano-structural properties. *Biomaterials*, 22(10), 1065–1075.
- Fields, R. D., Le Beau, J. M., Longo, F. M., & Ellisman, M. H. (1989). Nerve regeneration through artificial tubular implants. *Progress in Neurobiology*, 33(2), 87–134.
- Gonen-Wadmany, M., Goldshmid, R., & Seliktar, D. (2011). Biological and mechanical implications of PEGylating proteins into hydrogel biomaterials. *Biomaterials*, 32(26), 6025–6033.
- Herbert, C. B., Nagaswami, C., Bittner, G. D., Hubbell, J. A., & Weisel, J. W. (1998). Effects of fibrin micromorphology on neurite growth from dorsal root ganglia cultured in three-dimensional fibrin gels. *Journal of Biomedical Materials Research*, 40(4), 551–559.
- Isaacs, J. (2013). Major peripheral nerve injuries. *Hand Clinics*, 29(3), 371–382.
- Kehoe, S., Zhang, X. F., & Boyd, D. (2012). FDA approved guidance conduits and wraps for peripheral nerve injury: A review of materials and efficacy. *Injury*, 43(5), 553–572.
- Lee, A. C., Yu, V. M., Lowe, J. B., Brenner, M. J., Hunter, D. A., Mackinnon, S. E., & Sakiyama-Elbert, S. E. (2003). Controlled release of nerve growth factor enhances sciatic nerve regeneration. *Experimental Neurology*, 184(1), 295–303.
- Mironi-Harpaz, I., Berdichevski, A., & Seliktar, D. (2014). Fabrication of PEGylated fibrinogen: A versatile injectable hydrogel biomaterial. *Methods in Molecular Biology*, 1181, 61–68.
- Mironi-Harpaz, I., Wang, D. Y., Venkatraman, S., & Seliktar, D. (2012). Photopolymerization of cell-encapsulating hydrogels: Crosslinking efficiency versus cytotoxicity. *Acta Biomaterialia*, 8(5), 1838–1848.
- Mironi-Harpaz, I., Zigerson, S., & Seliktar, D. (2014). Fibrin-based hydrogel scaffolds for controlling cell-matrix interaction in vascular tissue engineering. *Advanced Biomaterials and Devices in Medicine*, 1, 78–87.
- Moy, O. J., Peimer, C. A., Koniuch, M. P., Howard, C., Zielezny, M., & Katikaneni, P. R. (1988). Fibrin seal adhesive versus nonabsorbable microsuture in peripheral nerve repair. *Journal of Hand Surgery. American Volume*, 13(2), 273–278.
- Peled, E., Boss, J., Bejar, J., Zinman, C., & Seliktar, D. (2007). A novel poly(ethylene glycol)-fibrinogen hydrogel for tibial segmental defect repair in a rat model. *Journal of Biomedical Materials Research. Part A*, 80(4), 874–884.
- Petterson, J., Kalbermatten, D., McGrath, A., & Novikovar, L. N. (2010). Biodegradable fibrin conduit promotes long-term regeneration after peripheral nerve injury in adult rats. *Journal of Plastic, Reconstructive & Aesthetic Surgery*, 63(11), 1893–1899.
- Platt, C. I., Krekoski, C. A., Ward, R. V., Edwards, D. R., & Gavrilovic, J. (2003). Extracellular matrix and matrix metalloproteinases in sciatic nerve. *Journal of Neuroscience Research*, 74(3), 417–429.
- Rufaihah, A. J., Johari, N. A., Vaibavi, S. R., Plotkin, M., Di Thien, D. T., Kofidis, T., & Seliktar, D. (2017). Dual delivery of VEGF and ANG-1 in ischemic hearts using an injectable hydrogel. *Acta Biomaterialia*, 48, 58–67.
- Rufaihah, A. J., Vaibavi, S. R., Plotkin, M., Shen, J. Y., Nithya, V., Wang, J., ... Kofidis, T. (2013). Enhanced infarct stabilization and neovascularization mediated by VEGF-loaded PEGylated fibrinogen hydrogel in a rodent myocardial infarction model. *Biomaterials*, 34(33), 8195–8202.
- Ryu, J. K., Davalos, D., & Akassoglou, K. (2009). Fibrinogen signal transduction in the nervous system. *Journal of Thrombosis and Haemostasis*, 7, 151–154.
- Sarig-Nadir, O., Livnat, N., Zajdman, R., Shoham, S., & Seliktar, D. (2009). Laser photoablation of guidance microchannels into hydrogels directs cell growth in three dimensions. *Biophysical Journal*, 96(11), 4743–4752.
- Sarig-Nadir, O., & Seliktar, D. (2008). Compositional alterations of fibrin-based materials for regulating in vitro neural outgrowth. *Tissue Engineering. Part A*, 14(3), 401–411.
- Sarig-Nadir, O., & Seliktar, D. (2010). The role of matrix metalloproteinases in regulating neuronal and nonneuronal cell invasion into PEGylated fibrinogen hydrogels. *Biomaterials*, 31(25), 6411–6416.
- Schmidt, C. E., & Leach, J. B. (2003). Neural tissue engineering: Strategies for repair and regeneration. *Annual Review of Biomedical Engineering*, 5, 293–347.
- Schmidt, O., Mizrahi, J., Elisseeff, J., & Seliktar, D. (2006). Immobilized fibrinogen in PEG hydrogels does not improve chondrocyte-mediated matrix deposition in response to mechanical stimulation. *Biotechnology and Bioengineering*, 95(6), 1061–1069.
- Sherman, D. L., & Brophy, P. J. (2005). Mechanisms of axon ensheathment and myelin growth. *Nature Reviews Neuroscience*, 6(9), 683–690.
- Shoichet, M. S., Tate, C. C., Baumann, M. D., & LaPlaca, M. C. (2008). Strategies for regeneration and repair in the injured central nervous system. In W. M. Reichert (Ed.), *Indwelling neural implants: Strategies for contending with the in vivo environment*. Boca Raton (FL).
- Spivey, E. C., Khaing, Z. Z., Shear, J. B., & Schmidt, C. E. (2012). The fundamental role of subcellular topography in peripheral nerve repair therapies. *Biomaterials*, 33(17), 4264–4276.
- Teuschl, A. H., Schuh, C., Halbweis, R., Pajer, K., Marton, G., Hopf, R., ... Hausner, T. (2015). A new preparation method for anisotropic silk fibroin nerve guidance conduits and its evaluation in vitro and in a rat sciatic nerve defect model. *Tissue Engineering. Part C, Methods*, 21(9), 945–957.
- Yoshii, S., Oka, M., Shima, M., Taniguchi, A., & Akagi, M. (2003). Bridging a 30-mm nerve defect using collagen filaments. *Journal of Biomedical Materials Research Part A*, 67a(2), 467–474.

**How to cite this article:** Berkovitch Y, Cohen T, Peled E, et al. Hydrogel composition and laser micropatterning to regulate sciatic nerve regeneration. *J Tissue Eng Regen Med*. 2018;12:1049–1061. <https://doi.org/10.1002/term.2606>